Spin Electronics

The Longitudinal Spin Seebeck Coefficient of Fe

Zhihao Duan[1], Bingfeng Miao[1,2], Liang Sun[1,2], Di Wu[1,2], Jun Du[1,2], and Haifeng Ding[1,2]

[1]National Laboratory of Solid State Microstructures, Department of Physics, Nanjing University, Nanjing 210093, China
[2]Collaborative Innovation Center of Advanced Microstructures, Nanjing University, Nanjing 210093, China

Received 25 Oct 2018, revised 3 Jan 2019, accepted 28 Jan 2019, published 4 Feb 2019, current version 1 Mar 2019.

Abstract—We report an experimental study of the longitudinal spin Seebeck effect (LSSE) of a Fe thin film with a Pt detection layer. By varying the Fe thickness, we find that the anomalous Nernst effect (ANE) of Fe changes sign and vanishes at about 4.8 nm. This provides a unique opportunity to study the LSSE where the influence of ANE is absent. The addition of a 3 nm Pt layer produces a considerable thermal voltage, which comes from the LSSE of Fe solely. The opposite signs of thermal voltages in Pt/Fe and W/Fe bilayer structures confirm that the signal is dominated by LSSE because Pt and W have opposite signs of spin Hall angle. In conjunction with the Pt-thickness-dependent measurement of effective spin-mixing conductance of Fe/Pt films, we estimate the spin Seebeck coefficient of Fe.

Index Terms—Spin electronics, anomalous Nernst effect, longitudinal spin Seebeck effect, spin Hall effect, spin Seebeck coefficient.

I. INTRODUCTION

The generation of pure spin current continues to play an important role in spintronics [Wolf 2001] and spin caloritronics [Bauer 2012]. Among various methods, the spin Seebeck effect (**SSE**) provides a versatile and easy route to convert thermal energy into a spin signal [Uchida 2008]. It has been demonstrated that SSE can be incorporated into thermoelectric and touch screen devices [Uchida 2014]. SSE refers to the spin version of the Seebeck effect. It describes the generation of pure spin current resulting from a temperature gradient. It can be measured in two geometries, i.e., the transverse SSE (**TSSE**) [Uchida 2008] and the longitudinal SSE (**LSSE**) [Uchida 2010a]. In TSSE, the temperature gradient is applied within the sample plane, and spin current diffuses perpendicularly to the sample plane into a material with large spin–orbit coupling such as Pt and results in an electrical voltage via the inverse spin Hall effect (**ISHE**) [Saitoh 2006]. TSSE has been reported in ferromagnetic conductors [Uchida 2008], insulators [Uchida 2010b], and semiconductors [Jaworski 2010], though there is still an ongoing debate about the existence of TSSE [Avery 2012, Schmid 2013]. In LSSE, both spin current and temperature gradient are along the out-of-plane direction [see Fig. 1(b)]. The obtained electric field is $\vec{E} \propto \vec{\sigma} \times \vec{J}_s$, where $\vec{\sigma}$ is the spin index parallel to the magnetization $\vec{M}$, and $\vec{J}_s$ is the pure spin current with its flow direction parallel to the temperature gradient ∇T. LSSE was demonstrated for the first time in a yttrium-iron-garnet (YIG)/Pt system [Uchida 2010a] and has been widely studied in various magnetic insulators where only magnon spin current is involved [Uchida 2010a, Kikkawa 2013b, Giles 2017]. Magnetic metals and semiconductors, however, are known to have anomalous Nernst effect (**ANE**) [Miyasato 2007, Pu 2008]. Under the out-of-plane temperature gradient, the ANE can be described by $\vec{E}_{\mathrm{ANE}} \propto \vec{M} \times \nabla T$ [see Fig. 1(a)]. Thus, it has exactly the same symmetry as LSSE. This makes them indistinguishable with respect to each other. Therefore, most studies of LSSE are limited to ferromagnetic insulators where the ANE is absent. Despite the fact that the ferromagnetic metals are commonly used in current spintronic devices, the detection and study of LSSE in them is still rare.

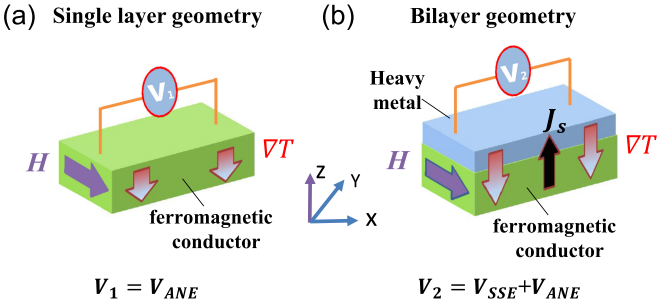

Fig. 1. Schematic illustrations of thermal voltage measurements under an external magnetic field. (a) FM single-layer geometry. (b) FM/heavy metal bilayer geometry. In (a), only a ferromagnetic layer is used, and the voltage corresponds to the ANE. In (b), a bilayer consisting a heavy metal and ferromagnetic layer is used. There is an additional contribution to the thermal voltage from the combined effect caused by LSSE and ISHE. Thus, the voltage signal is the sum of both.

Until very recently, only a few works began to discuss the LSSE in ferromagnetic metals. For instance, the LSSE in Permalloy (Py) (Ni_xFe_{100-x}) with zero contribution from ANE by tuning the ratio of Ni to Fe has been studied in Kannan [2017]. In Holanda [2017], the thermal signals of Py/NiO/Pt and Py/NiO/Ta trilayer structures have been studied, where NiO acts as a spin current channel but prevents the flow of charge current. The SSE coefficient as the ratio between charge current in the Pt layer with respect to the temperature gradient has been defined. One disadvantage of this definition is that it varies with the property of the FM-NM interface and NM material, where FM is the ferromagnet and NM is the nonmagnetic material. The same FM material would have different (even opposite sign) SSE coefficients when the NM layer/interface is different [Qu 2014]. The SSE coefficient, however, should be an intrinsic parameter of FM material itself. To resolve this issue, we characterize the SSE coefficient by the ratio between the generated spin current density in FM layer with respect to the temperature gradient. We present a

Corresponding authors: Bingfeng Miao and Haifeng Ding (e-mail: bfmiao@nju.edu.cn; hfding@nju.edu.cn).
Digital Object Identifier 10.1109/LMAG.2019.2897540

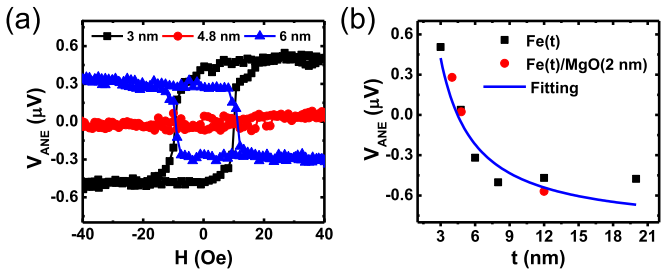

Fig. 2. (a) Magnetic-field-dependent V_{ANE} of Fe at three representative thicknesses. All data are obtained with $\Delta T = 12.6$ K applied along the $+z$-direction. (b) Fe-thickness dependence of the saturation value of V_{ANE}. Red circle/black square points are the ANE of Fe with and without MgO capping layer. The blue solid line shows a fitting using $V_{\mathrm{ANE}} = V^b_{\mathrm{ANE}} + (V_{\mathrm{ANE}}{}^s/t)$ with $V^b_{\mathrm{ANE}} = -0.86 \pm 0.13\mu$V and $V^s_{\mathrm{ANE}} = 3.85 \pm 0.81\mu$V, respectively.

quantitative study of LSSE in a single-element, ferromagnetic metal, ultrathin film of Fe. By varying the Fe thickness, ANE of Fe changes sign and vanishes at about 4.8 nm. The interface-induced ANE is also excluded by MgO- and Cu-capped control samples. The opposite sign of the thermal voltages in Pt/Fe and W/Fe bilayer structures also confirms that the signal is dominated by LSSE, since Pt and W have opposite sign in the spin Hall angle. Using Fe/Pt as an example system, we further characterize the effective spin-mixing conductance and interface spin loss (**ISL**) of the Pt-Fe interface by the ferromagnetic resonance (**FMR**) measurements of both Fe and Fe/Pt films. Assuming Pt does not significant change ANE of Fe, we estimate the spin Seebeck coefficient of Fe.

II. EXPERIMENTS AND RESULTS

In this letter, all samples are 5 mm × 0.2 mm stripes deposited onto 0.5 mm thick sapphire (0001) substrates by dc magnetron sputtering at a base pressure 2×10^{-5} Pa. Prior to the sputter deposition, the substrates are ultrasonically cleaned with acetone followed by ethanol and finally deionized water, all at the power of 100 W. The distance between the sputtering source and the substrate is around 65 mm. The deposition rates for all metals are ∼0.1 nm/s with Ar pressure ∼0.5–0.8 Pa. In order to avoid the oxidation of Fe, we performed all measurements in a dry atmosphere immediately after taking the samples out. Control samples with MgO and Cu capping are also performed. Both ends of the samples were connected to Cu electrodes with a separation of 4 mm for the voltage measurements via a Keithley nanovoltmeter 2182 A. The samples were placed in between an insulating resistance heater with the dimension of 40 mm × 12 mm and a large Cu block, which is maintained at room temperature. In such configuration, a stable vertical temperature gradient can be established and monitored with attached thermocouples. The in-plane temperature difference across the samples is smaller than 0.1 K, which is obtained by thermocouple.

The measured V_{ANE} of the Fe stripes as a function of the transverse magnetic field under vertical temperature gradient for three representative thicknesses is presented in Fig. 2(a). We note that the measured voltage may contain a small contribution of the SSE of Fe itself. The temperature difference ΔT across the whole sample is 12.6 K unless specified. Notice that 6 nm Fe exhibits a negative ANE at positive field with a magnitude of -0.31 ± 0.02 μV and reverses sign at negative field, which is consistent with the ANE of bulk Fe [Chuang 2017]. The exact value of the measured ANE voltage relies on the exact temperature gradient acting on Fe. Therefore, it is not surprising that our values are not in agreement to Chuang [2017] while the overall behavior is consistent. The ANE signal of 3 nm Fe shows the opposite behavior, which is positive at positive field, whereas for 4.8 nm Fe the ANE signal vanishes.

The V_{ANE} is negative and almost thickness independent for Fe films thicker than 8 nm [see Fig. 2(b)]. With decreasing t_{Fe}, V_{ANE} increases and crosses zero at ∼4.8 nm, and monotonously increases further with the thickness down to 3 nm. The sign reversal of ANE could be explained by the thickness-dependent Seebeck coefficient S_{xx} of Fe, as reported in Chuang [2017]. In general, the ANE-produced voltage $V_{\mathrm{ANE}} \propto \theta_{\mathrm{ANE}} S_{xx} \boldsymbol{M} \times \nabla T$ were θ_{ANE} is the ANE angle, $\boldsymbol{M}$ is the magnetization direction, and ∇T is the temperature gradient. When the film thickness is comparable to or less than the carrier mean free path, the Seebeck coefficient could be significantly influenced by surface scattering. This behavior can be described by the mean free path model $S_{xx}(t) = S_g(1 - b/t)$ [Pichard 1980], where S_g is the bulk Seebeck coefficient and b is the parameter related to surface and grain-boundary scattering. Therefore, the S_{xx} could change its sign when the film thickness is thin enough owing to significant surface scattering. Thus, we can also decompose the ANE signal into a bulk contribution V^b_{ANE} and a surface contribution V^s_{ANE} with $V^b_{\mathrm{ANE}} + (V_{\mathrm{ANE}}{}^s/t_{Fe})$ [Kannan 2017]. Fitting with this equation (blue curve) reproduces the experimental data with $V^b_{\mathrm{ANE}} = -0.86 \pm 0.13\mu$V and $V^s_{\mathrm{ANE}} = 3.85 \pm 0.81\mu$V, suggesting that the phenomenological model provides a reasonable description. The ANE data for Fe with or without a capping layer fall into almost the same curve [see Fig. 2(b)]. The ANE of Fe with 2 nm MgO capping layer vanishes at about the same thickness as for without MgO capping ∼ 4.8 nm, strongly suggesting a negligible influence of Fe oxidation at atmosphere. The absence of ANE is particularly important, since it provides an ideal platform for the study of LSSE in Fe.

In the following, we demonstrate the existence of LSSE in Fe(4.8 nm) where the influence of ANE in Fe is excluded. As shown in Fig. 3(a), Fe(4.8 nm)/Pt(3 nm) exhibits a positive thermal voltage of 0.55 ± 0.01 μV after saturation. The signal from Fe(4.8 nm)/Pt(3 nm) is significantly larger than that from Fe(4.8 nm), which is almost zero. The obtained thermal voltage from Fe(4.8 nm)/Pt(3 nm) is proportional to the temperature gradient [see Fig. 3(d)]. The sharp increase of thermal voltage in Fe(4.8 nm)/Pt(3 nm) is due to the spin current injected into Pt from LSSE in Fe. Reversing the growth sequence of Pt and Fe does not change any properties except a slight variation in coercivity [see Fig. 3(a)]. This is because the heat flow is always from top to bottom; meanwhile the spin current direction is also fixed. In a control sample, Fe(4.8 nm)/Cu(1 nm) exhibits negligible voltage < 0.03 μV, evidencing that the Fe-Cu interface has no ANE contribution [see Fig. 3(a)]. We also provide the atomic force microscopy images of Fe(4.8 nm) and Fe(4.8 nm)/Cu(1 nm) and both samples have roughness ∼0.1 nm; see Fig. 3(b) and (c). This proves that 1 nm of Cu is sufficient to separate Fe and Pt in Fe(4.8 nm)/Cu(1 nm)/Pt(3 nm) where a significant thermal voltage of 0.42 ± 0.02 μV was measured. As the upper and lower surface of Fe remain unchanged in Fe(4.8 nm)/Cu(1 nm)/Pt(3 nm) as compared with Fe(4.8 nm)/Cu(1 nm), the change of ANE is expected to be small. Thus, this validates that the thermal voltage in

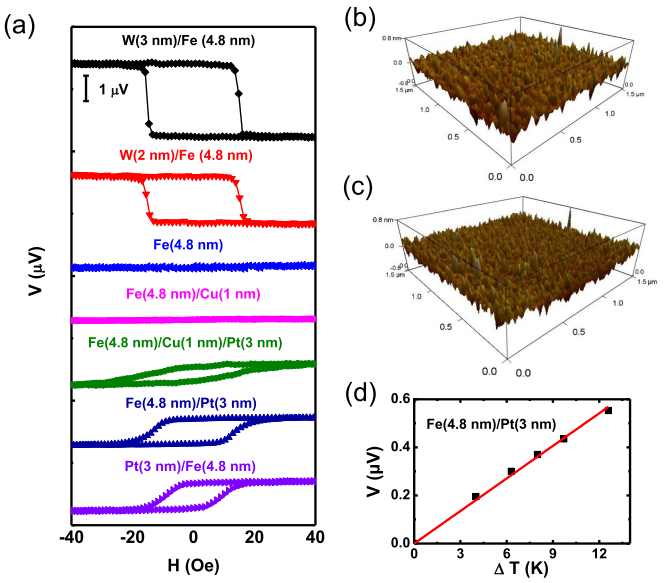

Fig. 3. (a) Comparison between the field dependence of thermal voltage at $\Delta T = 12.6$ K for various samples. The data have been shifted for clarity. (Right) Three-dimensional atomic force microscopy image of (b) Fe(4.8 nm) and (c) Fe(4.8 nm)/Cu(1 nm) on sapphire substrates. Both samples have similar roughness of ~0.1 nm. (d) ΔT dependence of V between the ends of the Fe(4.8 nm)/Pt(3 nm) wire, and the temperature difference is applied along the +z-direction.

Fe(4.8 nm)/Cu(1 nm)/Pt(3 nm) is indeed from LSSE in Fe, although the thermal voltage is slightly decreased compared to Fe(4.8 nm)/Pt(3 nm).

It is well known that W has a negative spin Hall angle [Pai 2012], implying that a reversed sign in thermal voltage should be obtained if W is the detecting layer. In order to obtain the beta-phase W that possesses a large spin Hall angle, we deposit W onto sapphire substrate. As expected, W(3 nm)/Fe(4.8 nm) and W(2 nm)/Fe(4.8 nm) exhibit negative voltages about -1.49 ± 0.02 μV and -0.98 ± 0.02 μV, respectively [see Fig. 3(a)]. The sign change of the thermal voltage between Pt/Fe and W/Fe also validates the existence of SSE in Fe.

In the following, we continue to discuss the quantification of the SSE coefficient of Fe, which was not addressed in previous studies. The SSE coefficient is defined as the amount of pure spin current density generation per unit temperature gradient, i.e., $S = J_{\rm SSE}/\nabla T_{Fe}$, where ∇T_{Fe} is the temperature gradient across the Fe layer. Taking into account the ISL and spin backflow from the Pt layer, the spin current density injected into the Pt layer at $t = 0$ nm can be described by [Chen 2015a, 2015b, Tao 2018]

$$J_S(0) = J_{\rm SSE}\left[1 - \frac{G^{\uparrow\downarrow}}{G^{\uparrow\downarrow} + \frac{2}{3}k_F^2\frac{l_{mf}}{\lambda_{sd}}\tanh(\frac{t_{Pt}}{\lambda_{\rm sd}})}\right](1-\delta)$$
$$= J_{\rm SSE}(1-\varepsilon)(1-\delta). \quad (1)$$

The term ε denotes the spin backflow factor in the Pt layer, δ is the parameter characterizing the ISL and is between 0 (no loss) and 1 (complete loss), $G^{\uparrow\downarrow}$ is the spin-mixing conductance of Pt-Fe interface, and $l_{\rm mf}$, $\lambda_{\rm sd}$, t_{Pt}= 3 nm, and $k_F = 5.7 \times 10^{10}$ m^{-1} [Deorani 2013] are the mean free path, spin diffusion length, thickness, and Fermi wave vector, all of the Pt layer, respectively. The spin-mixing conductance $G^{\uparrow\downarrow}$ can be calculated from the effective spin-mixing conductance, which is obtained through FMR measurements and will be discussed ahead [Chen 2015a, 2015b, Tao 2018]

$$g_{\rm eff}^{\uparrow\downarrow} = G^{\uparrow\downarrow}\left[1-(1-\delta)^2\varepsilon\right] \text{ with}$$
$$\varepsilon = G^{\uparrow\downarrow}/\left[G^{\uparrow\downarrow} + \frac{2}{3}k_F^2\frac{l_{mf}}{\lambda_{sd}}\tanh\left(\frac{t_N}{\lambda_{sd}}\right)\right]. \quad (2)$$

Due to spin diffusion and spin relaxation, the spin current decays away from the interface into the NM layer. Using the spin diffusion equation with the boundary condition $J_S(t = t_{\rm Pt}) = 0$ leads to a spin current density at position t as [Tserkovnyak 2005]

$$J_S(t) = J_S(0)\frac{\sinh[(t_{\rm Pt}-t)/\lambda_{\rm sd}]}{\sinh t_{\rm Pt}/\lambda_{\rm sd}}.$$

The charge current obtained via the ISHE is $J_C(t) = \theta_{\rm SH}\frac{2e}{\hbar}J_S(t)$, where $\theta_{\rm SH}$ is the spin Hall angle and $\hbar$ is the reduced Plank constant. By integrating the current along the Pt thickness, the thermal voltage can be obtained as

$$V_{\rm SSE} = J_S(0)\frac{2Rw\lambda_{\rm sd}e\theta_{\rm SH}\tanh\left(\frac{t_{\rm Pt}}{2\lambda_{\rm sd}}\right)}{\hbar} \quad (3)$$

where w and R are the width and the resistance of the sample, respectively. Therefore, in order to obtain the SSE coefficient of Fe, one also needs to know the values of $\theta_{\rm SH}$ and $\lambda_{\rm sd}$ of Pt, as well as the effective spin-mixing conductance $g_{\rm eff}^{\uparrow\downarrow}$ of the Pt-Fe interface.

The dynamic properties were studied utilizing FMR and spin rectification effect. The samples were placed on top of a coplanar waveguide, with an in-plane magnetic field H, and excited by a microwave field. Due to the anisotropic magnetoresistance, the electrical resistance also varied with time as the magnetization precessed. The time-dependent resistance multiplied by the induction current results in a spin rectification voltage. Fig. 4(a) shows the measured spin rectification voltage as a function of the in-plane field with an amplitude of A, where H is applied within the sample plane. By fitting it with the symmetrical Lorentzian function, we obtained the resonance field H_R and the linewidth ΔH, which is the half-width at half-maximum of the resonance peak. We performed similar measurements at different frequencies and obtained the frequency-dependent H_R [see solid symbols in Fig. 4(b)]. Fitting with the Kittel equation [see red line in Fig. 4(b)], we obtained the effective magnetization of Fe(4.8) as $4\pi M_s = 16.19 \pm 0.23$ kG. The damping factor α of Fe (Fe/Pt) can also be obtained from the linear fitting of the frequency-dependent ΔH through $\Delta H = \Delta H_0 + 2\pi\alpha f/\gamma$ [Mosendz 2009]; see Fig. 4(c). In the Fe/Pt bilayer, under the FMR condition, spin current is also pumped from Fe into Pt, resulting in an enhanced ΔH in comparison to that of the Fe single layer. The effective spin-mixing conductance of the Pt(3)-Fe interface

$$g_{\rm eff}^{\uparrow\downarrow} = \frac{4\pi M_s t_{\rm Fe}}{g\mu_B}(\alpha_{\rm Fe/Pt} - \alpha_{\rm Fe})$$

was calculated to be $(3.24 \pm 0.046) \times 10^{19}$ m^{-2}, which is similar to that reported in Papaioannou [2013]. In order to obtain the ISL parameter δ, we performed Pt-thickness measurement of $g_{\rm eff}^{\uparrow\downarrow}$ for Fe(4.8)/Pt(t). Fitting the curve with (2) yields $G^{\uparrow\downarrow} = (3.55 \pm 0.17) \times 10^{19}$ m^{-2}, $\delta = 0.06 \pm 0.06$, indicating that about 6% of the injected spin current is lost at the Pt-Fe interface.

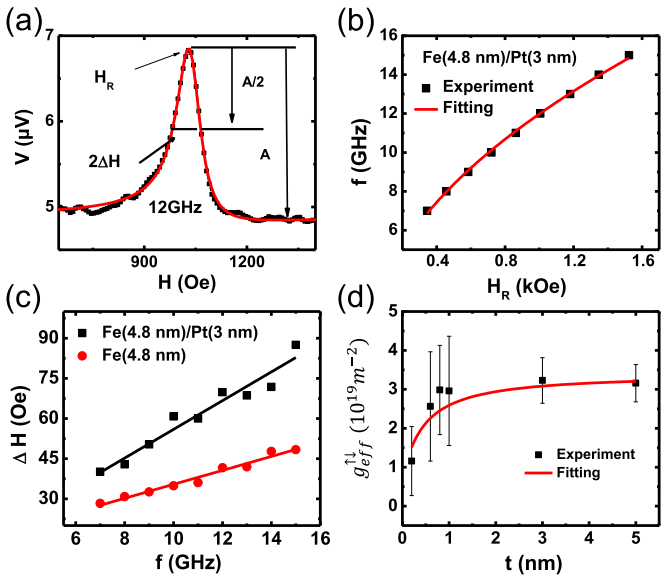

Fig. 4. (a) Typical spin rectification curve obtained at 12 GHz with the symmetrical Lorentzian function fitting in red curve. (b) Ferromagnetic resonance frequency versus magnetic field of Fe(4.8 nm)/Pt(3 nm) extracted from the spin rectification effect measurements. The solid line is the fitting using the Kittel equation. (c) FMR linewidth versus resonance frequency measured in Fe(4.8 nm)/Pt(3 nm) and Fe(4.8 nm). The solid lines are linear fittings.(d) Pt thickness dependence of the value of $g_{\text{eff}}^{\uparrow\downarrow}$. The red solid line shows a fitting using (2).

The resistances of Fe(4.8) and Fe(4.8)/Pt(3) are 2.92 and 1.41 kΩ, respectively. Through the shunting relationship, the resistivity of Pt was estimated to be $\sim 3.27 \times 10^{-7}$ Ω·m, and the mean free path was calculated to be 2.5 nm according to the Sommerfeld theory [Ashcroft 1976]. With the reported values of $\theta_{\text{SH}} = 0.03$ and $\lambda_{\text{sd}} = 8$ nm [Tao 2018], we further calculated the injected spin current density into the Pt layer to be $J_S(0) = (1.45 \pm 0.03) \times 10^{-11}$ J/m^2, and $\varepsilon = 0.064$ using (1)–(3), assuming Pt does not significant change ANE of Fe. Therefore, the generated spin current density within the Fe layer was estimated to be $J_{\text{SSE}} = (1.77 \pm 0.13) \times 10^{-11}$ J/m^2.

In order to quantify the SSE coefficient of Fe, the temperature difference across the Fe layer is still needed. This can be calculated by [Bergman 2011, Holanda 2017]

$$\Delta T_{\text{Fe}} = \frac{t_{\text{Fe}}/K_{\text{Fe}}}{t_{\text{Pt}}/K_{\text{Pt}} + t_{\text{Fe}}/K_{\text{Fe}} + t_{\text{Al}_2\text{O}_3}/K_{\text{Al}_2\text{O}_3}} \Delta T \approx \frac{K_{\text{Al}_2\text{O}_3} t_{\text{Fe}}}{K_{\text{Fe}} t_{\text{Al}_2\text{O}_3}} \Delta T$$

where t_{Pt}, t_{Fe}, and $t_{\text{Al}_2\text{O}_3}$ are the thicknesses of Pt and Al_2O_3, and K_{Pt}, K_{Fe}, and $K_{\text{Al}_2\text{O}_3}$ are the thermal conductivities of Pt, Fe, and Al_2O_3, respectively [Ashcroft 1976, Cahill 1998]. In it, the thermal conductance of the interface is assumed to be zero due to its ultrasmall thickness. As our transport was along the perpendicular direction, the surface scattering from the side walls can be neglected due to the large width (0.2 mm). Thus, we expect that the bulk thermal conductivity is a reasonable estimation for the perpendicular thermal conductivity. This approximation is also adopted in other perpendicular thermal transport experiments [Kikkawa 2013a, Holanda 2017]. Using $K_{Pt} = 67$ W/(m·K), $K_{Fe} = 80$ W/(m·K), and $K_{Al_2O_3} = 25$ W/(m·K) [Ashcroft 1976, Cahill 1998], we obtained the temperature gradient across Fe to be $\nabla T_{Fe} = 7.88$ K/mm. Thus, we could estimate the SSE coefficient of Fe to be $S = J_{\text{SSE}}/\nabla T_{Fe} = (2.25 \pm 0.16) \times 10^{-15}$ J/(m·K).

III. DISCUSSION

Due to the very weak spin–orbit coupling of Cu and our limited experimental sensitivity, we could not measure the spin loss of the Fe/Cu/Pt trilayer system directly at the present stage. Instead, we estimated it by comparing the amplitude of the converted charge current (the obtained thermal voltage divided by the resistance) of Fe/Pt(3 nm) and Fe/Cu(1 nm)/Pt(3 nm) (1.26 kΩ). Considered the spin loss of Fe/Pt is 0–12%, the estimated spin loss in Fe/Cu(1 nm)/Pt(3 nm) is 9–30%, which qualitatively agrees with the reported 26–78% for Co/Cu(5 nm)/Pt in Rojas-Sánchez [2014].

It is also interesting to compare the SSE coefficient of Fe with that of YIG. A value of $V_{\text{LSSE}} = 10$ μV for 3 nm Pt on YIG slab with the length $L = 5$ mm under $\nabla T = 20$ K/mm, namely, $V_{\text{LSSE}}/(L \cdot \nabla T) = 0.1$ μV/K, has been reported in Miao [2014]. A similar value is reported in Guo [2016], where the authors found $V_{\text{LSSE}}/(L \cdot \nabla T) < 0.3$ μV/K at room temperature. In this letter, $V_{\text{LSSE}} = 0.55 \pm 0.01$ μV for Fe(4.8 nm)/Pt(3 nm) with temperature gradient $\nabla T \approx 7.88$ K/mm and length 4 mm. After considering the shunting effect, $V_{\text{LSSE}}/(L \cdot \nabla T) \approx 0.034$ μV/K. If we assume the FM-NM interface properties are the same, the spin Seebeck coefficient of YIG is estimated to be ~3–9 times of that of Fe.

In summary, we present a quantitative study of the LSSE of a Fe thin film. With decreasing Fe film thickness, the ANE vanishes at 4.8 nm. By fixing the Fe film thickness at 4.8 nm and adding a Pt layer, we demonstrate the LSSE of Fe, without the influence of ANE. Consistent with the LSSE and ISHE theory, the thermal voltages change sign for Pt and W detecting layers. In combination with the spin-mixing conductance of the Pt-Fe interface, we find that the ISL is ~6% and the estimated SSE coefficient of Fe is $(2.25 \pm 0.16) \times 10^{-15}$ J/(m·K).

ACKNOWLEDGMENT

This work was supported in part by the National Key R&D Program of China under Grant 2018YFA0306004 and Grant 2017YFA0303202; in part by the National Natural Science Foundation of China under Grant 51601087, Grant 51571109, Grant 11734006, Grant 11727808, and Grant 51471085; in part by the Natural Science Foundation of Jiangsu Province under Grant BK20150565; and in part by the Fundamental Research Funds for the Central Universities under Grant 020414380078 and Grant 020414380104. The authors thank Mr. P. Omelchenko for careful reading and improving this letter.

REFERENCES

Ashcroft N W, Mermin N D (1976), "The Sommerfeld theory of metals," in *Solid State Physics*. Philadelphia, PA, USA: Saunders College, ch. 2.

Avery A D, Pufall M R, Zink B L (2012), "Observation of the planar Nernst effect in Permalloy and nickel thin films with in-plane thermal gradients," *Phys. Rev. Lett.*, vol. 109, 196602, doi: 10.1103/PhysRevLett.109.196602.

Bauer G E W, Saitoh E, van Wees B J (2012), "Spin caloritronics," *Nature Mater.*, vol. 11, pp. 391–399, doi: 10.1038/nmat3301.

Bergman T L, Incropera F P, DeWitt D P, Lavine A S (2011), "Introduction to conduction," in *Fundamentals of Heat and Mass Transfer*. Hoboken, NJ, USA: Wiley, ch. 2.

Cahill D G, Lee S-M, Selinder T I (1998), "Thermal conductivity of κ-Al_2O_3 and α-Al_2O_3 wear-resistant coatings," *J. Appl. Phys.*, vol. 83, pp. 5783–5786, doi: 10.1063/1.367500.

Chen K, Zhang S (2015a), "Spin pumping in the presence of spin-orbit coupling," *Phys. Rev. Lett.*, vol. 114, 126602, doi: 10.1103/PhysRevLett.114.126602.

Chen K, Zhang S (2015b), "Spin pumping induced electric voltage," *IEEE Magn. Lett.*, vol. 6, 3000304, doi: 10.1109/LMAG.2015.2427120.

Chuang T C, Su P L, Wu P H, Huang S Y (2017), "Enhancement of the anomalous Nernst effect in ferromagnetic thin films," *Phys. Rev. B*, vol. 96, 174406, doi: 10.1103/PhysRevB.96.174406.

Deorani P, Yang H (2013), "Role of spin mixing conductance in spin pumping: Enhancement of spin pumping efficiency in Ta/Cu/Py structures," *Appl. Phys. Lett.*, vol. 103, 232408, doi: 10.1063/1.4839475.

Giles B L, Yang Z, Jamison J S, Gomez-Perez J M, Vélez S, Hueso L E, Casanova F, Myers R C (2017), "Thermally driven long-range magnon spin currents in yttrium iron garnet due to intrinsic spin Seebeck effect," *Phys. Rev. B*, vol. 96, 180412, doi: 10.1103/PhysRevB.96.180412.

Guo E-J, Cramer J, Kehlberger A, Ferguson C A, MacLaren D A, Jakob G, Kläui M (2016), "Influence of thickness and interface on the low-temperature enhancement of the spin Seebeck effect in YIG films," *Phys. Rev. X*, vol. 6, 031012, doi: 10.1103/PhysRevX.6.031012.

Holanda J, Santos O A, Cunha R O, Mendes J B S, Rodríguez-Suárez R L, Azevedo A, Rezende S M (2017), "Longitudinal spin Seebeck effect in permalloy separated from the anomalous Nernst effect: Theory and experiment," *Phys. Rev. B*, vol. 95, 214421, doi: 10.1103/PhysRevB.95.214421.

Jaworski C M, Yang J, Mack S, Awschalom D D, Heremans J P, Myers R C (2010), "Observation of the spin-Seebeck effect in a ferromagnetic semiconductor," *Nature Mater.*, vol. 9, pp. 898–903, doi: 10.1038/nmat2860.

Kannan H, Fan X, Celik H, Han X, Xiao J Q (2017), "Thickness dependence of anomalous Nernst coefficient and longitudinal spin Seebeck effect in ferromagnetic Ni_xFe_{100-x} films," *Sci. Rep.*, vol. 7, 6175, doi: 10.1038/s41598-017-05946-1.

Kikkawa T, Uchida K, Daimon S, Shiomi Y, Adachi H, Qiu Z, Hou D, Jin X-F, Maekawa S, Saitoh E (2013a), "Separation of longitudinal spin Seebeck effect from anomalous Nernst effect: Determination of origin of transverse thermoelectric voltage in metal/insulator junctions," *Phys. Rev. B*, vol. 88, 214403, doi: 10.1103/PhysRevB.88.214403.

Kikkawa T, Uchida K, Shiomi Y, Qiu Z, Hou D, Tian D, Nakayama H, Jin X-F, Saitoh E (2013b), "Longitudinal spin Seebeck effect free from the proximity Nernst effect," *Phys. Rev. Lett.*, vol. 110, 067207, doi: 10.1103/PhysRevLett.110.067207.

Miao B F, Huang S Y, Qu D, Chien C L (2014), "Physical origins of the new magnetoresistance in Pt/YIG," *Phys. Rev. Lett.*, vol. 112, 236601, doi: 10.1103/PhysRevLett.112.236601.

Miyasato T, Abe N, Fujii T, Asamitsu A, Onoda S, Onose Y, Nagaosa N, Tokura Y (2007), "Crossover behavior of the anomalous Hall effect and anomalous Nernst effect in itinerant ferromagnets," *Phys. Rev. Lett.*, vol. 99, 086602, doi: 10.1103/PhysRevLett.99.086602.

Mosendz O, Woltersdorf G, Kardasz B, Heinrich B, Back C H (2009), "Magnetization dynamics in the presence of pure spin currents in magnetic single and double layers in spin ballistic and diffusive regimes," *Phys. Rev. B*, vol. 79, 224412, doi: 10.1103/PhysRevB.79.224412.

Pai C-F, Liu L, Li Y, Tseng H W, Ralph D C, Buhrman R A (2012), "Spin transfer torque devices utilizing the giant spin Hall effect of tungsten," *Appl. Phys. Lett.*, vol. 101, 122404, doi: 10.1063/1.4753947.

Papaioannou E T, Fuhrmann P, Jungfleisch M B, Brächer T, Pirro P, Lauer V, Lösch J, Hillebrands B (2013), "Optimizing the spin-pumping induced inverse spin Hall voltage by crystal growth in Fe/Pt bilayers," *Appl. Phys. Lett.*, vol. 103, 162401, doi: 10.1063/1.4825167.

Pichard C R, Tellier C R, Tosser A J (1980), "Thermoelectric power of thin polycrystalline metal films in an effective mean free path model," *J. Phys. F: Metal Phys.*, vol. 10, pp. 2009–2014, doi: 10.1088/0305-4608/10/9/016.

Pu Y, Chiba D, Matsukura F, Ohno H, Shi J (2008), "Mott relation for anomalous Hall and Nernst effects in $Ga_{1-x}Mn_xAs$ ferromagnetic semiconductors," *Phys. Rev. Lett.*, vol. 101, 117208, doi: 10.1103/PhysRevLett.101.117208.

Qu D, Huang S Y, Miao B F, Huang S X, Chien C L (2014), "Self-consistent determination of spin Hall angles in selected 5d metals by thermal spin injection," *Phys. Rev. B*, vol. 89, 140407, doi: 10.1103/PhysRevB.89.140407.

Rojas-Sánchez J-C, Reyren N, Laczkowski P, Savero W, Attané J-P, Deranlot C, Jamet M, George J-M, Vila L, Jaffrès H (2014), "Spin pumping and inverse spin Hall effect in platinum: The essential role of spin-memory loss at metallic interfaces," *Phys. Rev. Lett.*, vol. 112, 106602, doi: 10.1103/PhysRevLett.112.106602.

Saitoh E, Ueda M, Miyajima H, Tatara G (2006), "Conversion of spin current into charge current at room temperature: Inverse spin-Hall effect," *Appl. Phys. Lett.*, vol. 88, 182509, doi: 10.1063/1.2199473.

Schmid M, Srichandan S, Meier D, Kuschel T, Schmalhorst J-M, Vogel M, Reiss G, Strunk C, Back C H (2013), "Transverse spin Seebeck effect versus anomalous and planar Nernst effects in Permalloy thin films," *Phys. Rev. Lett.*, vol. 111, 187201, doi: 10.1103/PhysRevLett.111.187201.

Tao X, Liu Q, Miao B, Yu R, Feng Z, Sun L, You B, Du J, Chen K, Zhang S, Zhang L, Yuan Z, Wu D, Ding H F (2018), "Self-consistent determination of spin Hall angle and spin diffusion length in Pt and Pd: The role of the interface spin loss," *Sci. Adv.*, vol. 4, eaat1670, doi: 10.1126/sciadv.aat1670.

Tserkovnyak Y, Brataas A, Bauer G E W, Halperin B I (2005), "Nonlocal magnetization dynamics in ferromagnetic heterostructures," *Rev. Mod. Phys.*, vol. 77, pp. 1375–1421, doi: 10.1103/RevModPhys.77.1375.

Uchida K, Adachi H, Ota T, Nakayama H, Maekawa S, Saitoh E (2010a), "Observation of longitudinal spin-Seebeck effect in magnetic insulators," *Appl. Phys. Lett.*, vol. 97, 172505, doi: 10.1063/1.3507386.

Uchida K, Ishida M, Kikkawa T, Kirihara A, Murakami T, Saitoh E (2014), "Longitudinal spin Seebeck effect: From fundamentals to applications," *J. Phys.: Condens. Matter*, vol. 26, 343202, doi: 10.1088/0953-8984/26/34/343202.

Uchida K, Takahashi S, Harii K, Ieda J, Koshibae W, Ando K, Maekawa S, Saitoh E (2008), "Observation of the spin Seebeck effect," *Nature*, vol. 455, pp. 778–781, doi: 10.1038/nature07321.

Uchida K, Xiao J, Adachi H, Ohe J, Takahashi S, Ieda J, Ota T, Kajiwara Y, Umezawa H, Kawai H, Bauer G E W, Maekawa S, Saitoh E (2010b), "Spin Seebeck insulator," *Nature Mater.*, vol. 9, pp. 894–897, doi: 10.1038/nmat2856.

Wolf S A, Awschalom D D, Buhrman R A, Daughton J M, von Molnár S, Roukes M L, Chtchelkanova A Y, Treger D M (2001), "Spintronics: A spin-based electronics vision for the future," *Science*, vol. 294, pp. 1488–1495, doi: 10.1126/science.1065389.